doi:10.1111/j.1558-5646.2009.00737.x

GENETIC ANALYSIS OF SKULL SHAPE VARIATION AND MORPHOLOGICAL INTEGRATION IN THE MOUSE USING INTERSPECIFIC RECOMBINANT CONGENIC STRAINS BETWEEN C57BL/6 AND MICE OF THE *MUS SPRETUS* SPECIES

Gaëtan Burgio,[1,2,3,4] Michel Baylac,[5,6] Evelyne Heyer,[2,7] and Xavier Montagutelli[1,8]

[1]*Unité postulante de Génétique fonctionnelle de la Souris, CNRS URA 2578, Institut Pasteur, 25-28 rue du Docteur Roux 75724 Paris cedex 15, France*

[2]*Unité d' Eco-Anthropologie "Equipe génétique des populations humaines," CNRS MNHN P7, UMR 5145, Musée de l'Homme, 16 place du Trocadéro 75116 Paris, France*

[3]*Menzies Research Institute, University of Tasmania, Private bag 109, 7005 Hobart, Tasmania, Australia*

[4]*E-mail: grburgio@utas.edu.au*

[5]*Origine, structure et évolution de la biodiversité, UMR5202 et Plate-forme Morphométrie, MNHN, CNRS IFR 101, UMR 5202, Laboratoire d'Entomologie du Muséum National d'Histoire Naturelle, 45 rue Buffon 75005 Paris, France*

[6]*E-mail: baylac@mnhn.fr*

[7]*E-mail: heyer@mnhn.fr*

[8]*E-mail: xmonta@pasteur.fr*

Received October 6, 2008
Accepted April 21, 2009

To assess the genetic basis of the skull shape variation and morphological integration in mice, we have used a tool based on the cross between the distantly related mouse species *Mus spretus* (SEG/Pas strain) and the laboratory strain C57BL/6 called interspecific recombinant congenic strains (IRCSs). The genome of each IRCS consists on average of 1.3% of SEG/Pas derived sequences, located on multiple chromosomes as small-sized, DNA segments. Quantitative trait loci (QTL) on the skull shape, separated into dorsal and ventral sides, were analyzed in 17 IRCSs by a Procrustes superimposition method using 3D landmarks. The shapes of 16 strains differed significantly from C57BL/6. Discrepancy in the QTLs effects was found between the dorsal side and the anterior region of the ventral side due to a differential effect of the SEG/Pas alleles on the skull shape. A comprehensive analysis of all allelic combinations of the BCG-66H strain showed strong epistatic interactions between SEG/Pas segment acting on both skull sides. Epistatic pleiotropy and covariation between sides were dependent in SEG/Pas alleles direction and contributed to the strong morphological integration between sides. Introduction of *Mus spretus* alleles in a C57BL/6 background induced strong morphological changes mostly in SEG/Pas alleles direction and provided evidence for high level of morphological integration.

KEY WORDS: **Covariation between traits, epistasis, fluctuating asymmetry, pleiotropy, Procrustes superimposition, quantitative trait loci.**

An essential requirement in understanding the evolution of organisms form is the knowledge of the genetic basis of shape variation. Studies of the genetic control of variation for complex morphological features have used various model organisms including cichlid fish (Albertson et al. 2005), butterfly (Beldade et al. 2002), *Drosophila* (Liu et al. 1996; Laurie et al. 1997; Zeng et al. 2000; Mezey et al. 2005), plants (Langlade et al. 2005), and inbred strains of mice (Cheverud et al. 1997; Shimizu et al. 2004). Mouse models have been widely used in the past decade to address the question of the genetic variation in morphological integration and to understand the evolutionary basis of complex traits (Cheverud et al. 1997; Leamy et al. 1997, 1999; Klingenberg et al. 2001, 2004). The theory of the morphological integration is defined by the evolution of related phenotypic traits as a unit (Olson and Miller 1958). One approach to investigate this theory is to study the covariation between traits and to assess its inheritance. A genetic basis for morphological integration was first established by Lande (1979). He showed that evolution of related traits is driven by the degree of their functional or developmental relationships. Recently, quantitative trait loci (QTL) mapping methods have provided a powerful way to understand the pattern of genetic variation in morphological integration (e.g., Cheverud et al. 1997; Leamy et al. 1997, 1999; Klingenberg et al. 2001, 2004). These studies indicated that pleiotropic effects of QTLs and described a modular organization of the skull (Leamy et al. 1999) or of the mandible (Cheverud et al. 1997, 2004; Ehrich et al. 2003). However, Procrustes superimposition on the mandible with the same dataset did not confirm the latter finding (Klingenberg et al. 2004). Only limited sets of experiments have explored the genetic basis of the covariation and pleiotropy on the shape of the skull. Most have been performed using the same experimental data generated from an intercross between LG/J and SM/J strains of mice (Leamy et al. 1999, Wolf et al. 2005). A QTL-mapping analysis on nine cranial measurements by Leamy et al. (1999) identified 26 QTLs with significant additive effects. Two distinct pleiotropic patterns on the cranial vault and the face were distinguished corresponding to the early and late developmental areas (Leamy et al. 1999). Additionally, Wolf et al. (2005) demonstrated that the pleiotropic effect of epistasis (also referred as epistatic pleiotropy) is also an important source of covariation between traits and contributes positively in the genetic variation of morphological integration (Wolf et al. 2005, 2006). However, little is known about the spatial patterning of the QTLs effects, the evolutionary direction of epistasic pleiotropy, or the covariance between skull shape traits. These previous studies used only nine cranial measurements (Leamy et al. 1999; Wolf et al. 2005) and unfortunately they were not sufficient to cover all the complexities of the skull shape morphology and to investigate the pleiotropic pattern of the QTLs effects on the skull shape in direct relation with anatomy.

The concept of geometry for shape separated the statistical treatment for size and shape. Consequently, phenotype modification is described in direct relation with anatomical changes. All the previous studies on QTL mapping with geometric morphometrics methods have been performed on 2D-landmarks, mostly on the mouse mandible (Klingenberg et al. 2001, 2004) or on molar characters (Workman et al. 2002) using the two-generation crosses between two classical inbred strains of mice (LG/J × SM/J). There is no information on the genetic architecture of skull shape in three dimensions. Moreover, all the previous studies with 3D landmarks have been performed on mutant mice by 3D scanning reconstruction (Willmore et al. 2006b; Young et al. 2007) using Procrustes superimposition (Willmore et al. 2006b; Hallgrimsson et al. 2006, 2007) or Euclidean distances based (Willmore et al. 2006a; Hill et al. 2007).

Genetic analysis of complex traits also requires phenotypic and genotypic polymorphism. All inbred strains of mice used today stem from three subspecies of the genus *Mus*: *Mus musculus domesticus* (the occidental wild mice), *Mus musculus musculus* (the oriental wild mice), and *Mus castaneus* (the Asiatic wild mice) with a variable proportion of the three founders in the genome (e.g., *M. m. domesticus* [90%], *M. m. musculus* [5 to 7%] and *M. castaneus* [less than 2%] [Wade et al. 2002; Yang et al. 2007]). Although most of the genetic studies involving mice model have used classical laboratory strains, the use of wild-derived inbred strains has also proven valuable by providing relatively higher levels of genotypic and phenotypic variations (Guénet and Montagutelli 1994; Guénet and Bonhomme 2003) and DNA sequence (Ideraabdullah et al. 2004). *Mus spretus* is a western Mediterranean short-tailed mouse that emerged 2.5 million years ago (Guénet and Bonhomme 2003). It is sympatric with *M. m. domesticus* and but has rarely produced hybrids in nature (Guénet and Bonhomme 2003). *Mus spretus* species exhibits a high level of genetic and phenotypic polymorphism compared with the classical inbred strains of mice, in the same order of magnitude as that between human and chimpanzee (Newman et al. 2005). *Mus spretus* species also proved particularly useful in genetic-based studies investigating carcinogenesis (van Wezel et al. 1996; Nagase et al. 2001; Santos et al. 2002), fertility (Montagutelli et al. 1996; Zechner et al. 1996; Hemberger et al. 2001), responses to infectious diseases (Min-Oo et al. 2003), and was used to generate the first high-density genetic map for the mouse (Breen et al. 1994).

RCSs have been developed as a useful tool to help dissect polygenic traits (Demant and Hart 1986). In theory, with three backcrosses in a series of 20 RCSs, each strain carries 12.5% of its genome from a donor strain, and 87.5% from a recipient strain to cover 91% of the donor genome (Demant and Hart 1986). In a panel of donor strain segments with nonoverlapping segment in each RCS, therefore, the complex trait of interest become

distributed into different RCSs with nonlinked segments in which they can be analyzed one by one. Hence, the RCS system transformed a complex trait into a series of single gene traits, where each gene contributing to the polygenic trait could be mapped and studied separately (Demant and Hart 1986). Genetic factors for a number of traits have been discovered using RCSs (Moen et al. 1991; Morel et al. 1997), as well as epistatic interactions (Morel et al. 2000). Although all existing sets have been developed between inbred strains of mice, we have combined this strategy with the very high polymorphism rate inherent to interspecific crosses. Recently, we established a set of 55 interspecific recombinant congenic strains (IRCSs) with the *Mus spretus*-derived SEG/Pas (SEG) strain as a donor, and C57BL/6 (B6) as a recipient strain (Burgio et al. 2007). This collection carries between 0 and 3.8% (average 1.37%) of the SEG genome on a B6 background (Burgio et al. 2007). *M spretus* genome segments were distributed as a few chromosomal segments with an average size of 11 Mb. The proportion of the SEG genome represented by the 55 strains was 45.6%. The major reduction of *M. spretus* genome coverage compared to the expectations based was due to counter-selection against *M. spretus* alleles. Despite the limited number of IRCSs and a resolution map with an 11 Mb average size, compared with segregating populations such as F2s or outbred population based crosses (heterogenous stocks of mice, [Mott and Flint 2002; Valdar et al. 2006]), in which every individual carries a unique genotype, RCSs allow for replications and a trait can be measured on a group of genetically identical, sex- and age-matched individuals, buffering between-individual noise (for a full discussion on resolution map and comparison between IRCSs and other existing resources in mice see Burgio et al. 2007).

In this study, we intended to identify new QTLs associated with skull shape variation and asymmetry (fluctuating and directional asymmetry) and the relation between QTLs effects, morphological integration, and pleiotropy. For this purpose, we used an original model of 17 IRCSs with six allelic combinations for one IRCS and 3D landmarks associated with Procrustes superimposition on the skull shape.

Materials and Methods

MICE

IRCSs were developed at the Institut Pasteur in Paris (Burgio et al. 2007). Wild-derived inbred strain SEG/Pas (*Mus spretus*) males, the donor strain, were mated to C57BL/6J laboratory strain (B6) females (Charles Rivers Laboratories, L'Arbresle, France), the recipient strain, to produce F1 females and then breed with B6 males to produce an N2 generation. Fertile N2 males were then crossed with B6 females and their progeny were brother–sister mated for over 20 generation to produce inbred strains. Fifty-five strains were derived from their progeny. Majority of strains carry 2% of *SEG* genome into B6 background. Full description of these strains is available at http://www.pasteur.fr/recherche/unites/Gfons/ircs/ircshome.htm. To study allelic effects of the BcG-66H (containing three chromosomal SEG/Pas segments), (66HxB6)F1 male was mated with B6 females to produce two backcrosses generation from which each of the three chromosomal regions was isolated by genotyping and selecting the mice. Intercrossing monocongenic strains produced bicongenic strains. All animals were raised in the same animal room, under a 12 h : 12 h light : dark cyle, and received the same food (A03/10 pellets, SAFE, Augy, France). Pups were weaned at 4 weeks of age. Up to four male mice of the same litter were grouped. All protocols were in agreement with the Institut Pasteur guidelines for experiments on live vertebrates.

The set of IRCS was named BcG. Each strain was named after the number of the fertile N2 male it was derived from, followed by a letter indicating the strain order. For example, BcG-122C was the third strain derived from the 122 N2 male. However, for simplicity, it is often referred to simply as 122C. IRCSs were genotyped three times at different stages of inbreeding. IRCS animals were genotyped for 490 single nucleotide polymorphisms (SNP) and 183 microsatellites. Individual DNAs were prepared by standard phenol–chloroform extraction from tails. Microsatellite markers were genotyped according to standard polymerase chain reaction (PCR) protocols and SNP markers were genotyped by pyrosequencing according to the pyrosequencer manufacturer's recommendations (Biotage, Uppsala, Sweden). All the details on the genotyping methodology were described previously (Burgio et al. 2007). The presence of the three chromosomal segments carried by strain 66H was assessed using the following markers located close to the boundaries of each segment. Chromosome 1: *D1Mit81* (87.599477 Mb) and *rs6259837* (119.094898 Mb); chromosome 13: *D13Mit106* (93.838592 Mb) and *D13Mit290* (103.968912 Mb); chromosome 18: *D18Mit23* (42.783975 Mb) and *D18Mit123* (56.096090 Mb). A total of 554 males mice were retained for analysis divided in 379 individuals for the IRCSs and 175 mice of six allelic combinations of 66H corresponding to a minimum of 15 male mice per strains. Two repetitions of measures on the dorsal and ventral side of the skull were taken from a subsample of 296 mice comprising all IRCSs. Complete count of the IRCSs is indicated in Table 1.

SKULL PREPARATION AND DATA ACQUISITION

All mice analyzed for skull morphology were 60 $\pm$ 5 days old males. They were euthanized by CO_2 asphyxiation. The head was separated from the body and fixed in 100% ethanol for one week and the soft tissues were manually dissected. The skull was then immersed in 12% sodium hypochlorite for 30 minutes, rinsed with water for 10 minutes and dried for 6 hours. To examine the skull shape variation, we used landmark-based geometric shape

Table 1. Number of mice, size, number of SEG segments and number of genes per IRCSs.

Strains	No. of mice	Size of SEG genome	No. of SEG segments	No. of genes
C57BL/6	19			
5A	23	70.7	2	820
6A	19	65	3	594
6C	28	92.28	5	713
49A	15	65.75	3	546
66H	25	51.31	3	312
103E	15	37.82	4	324
119H	24	42.3	2	456
120C	24	108.5	5	850
122C	22	46.12	2	429
122D	18	73.19	4	937
122F	17	21.79	2	257
135B	21	49.58	2	333
135E	21	17.41	1	186
137E	19	17.1	1	192
137F	19	46.01	2	366
137G	21	27.38	2	264
157F	15	40.61	2	455
SEG	14			
Total	379			
66H-Chr1	31	30.3	1	151
66H-Chr13	31	7.7	1	79
66H-Chr18	33	13.31	1	82
66H-Chr13+18	30	21.01	2	161
66H-Chr1+13	28	38	2	230
66H-Chr1+18	22	43.61	2	233
Total	175			

The size of SEG genome and the number of SEG segments were determined both by microsatellites and SNP genotyping. A number of genes were assessed by the Mouse Genome Informatics website (http://www.informatics.jax.org/genes.shtml)

analysis. Three-dimensional landmarks were acquired with a Reflex microscope (Reflex Inc, Cambridge, U.K.). Full descriptions of the landmarks are shown in Figure 1 and Table 2. We defined 22 homologous landmarks on the dorsal side of the skull including the face and the cranial vault, and 19 homologous landmarks on the ventral side of the skull including the basicranium and the inferior part of the maxilla associated with the palatine bone.

PROCRUSTES SUPERIMPOSITION

To analyze the shape changes corresponding to the QTL effects and to interpret them in direct relation to the anatomy of the skull, we used geometric morphometric methods. Geometric morphometric methods are based on the geometric definition of shape. The skull is described by 3D-landmark configurations, localized

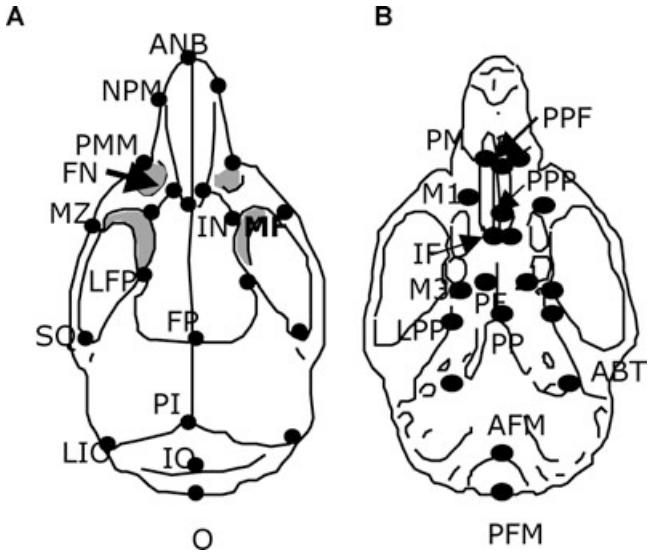

Figure 1. Landmarks sampled on IRCS skulls: (A) dorsal side, (B) ventral side. Abbreviations and full description of landmarks are given in the Table 1.

on invariant anatomical structures (Bookstein 1991; Dryden and Mardia 1998). We performed a generalized Procrustes analysis (GPA) (Bookstein 1996; Dryden and Mardia 1998) associated with the generalized least square method. Points were translated, normalized by centroid size (square root of the sum of squared distances between the centroid location and all landmarks of an object), and rotated to minimize the sum of squared distances between the mean conformations (consensus) (Dryden and Mardia 1998). Thus, the superimposed coordinates were projected onto the tangent space shape that is analogous to the projection of the curved surface of the earth onto a flat map (Rohlf 1999). The coordinates resulting from the Procrustes superimposition and projection onto the tangent shape space contained all the information of shape variability. To investigate the control of QTLs effects on symmetry and asymmetry, we separated the statistical treatment of shape among individuals into the symmetric and the asymmetric components, that is, the variation in the left–right averages of a trait, from the left–right asymmetries within individuals. Conformations of the superimposed coordinates for every individual were reduced to the symmetric and the asymmetric part using the object symmetry procedure (Mardia et al. 2000; Klingenberg et al. 2002), which consists in copying a reflected configuration (by reversing the signs of the X coordinates of each landmark). Then, landmarks on the left and right side of the median axis of the reflect copy are relabeled. Thus, the original and reflected conformations are superimposed and the symmetric component corresponds to the mean point between the original and the reflected configuration. Previous studies (Leamy et al. 1997; Klingenberg et al. 2001) distinguished two types of left–right asymmetry that can be measured for individuals: signed and unsigned

Table 2. Landmarks recorded in mice skulls using a three-dimensional reflex microscope (Reflex*).

Landmark	Description	Position
Dorsal side		
ANB	anteriormost point of the nasal bone	medial
NPM	junction between nasal bone and premaxilla	lateral
PMM	junction between premaxilla and maxilla	lateral
IN	suture between nasal and interfrontal bone	medial
FN	suture between posteriormost nasal and frontal bone	lateral
MF	suture between maxilla and frontal bone	lateral
MZ	suture between maxilla and zygomatic bone	lateral
FP	suture frontoparietal	medial
LFP	suture between lateral part of the frontal and parietal bone	lateral
PI	suture between parietal and interparietal bone	medial
IO	posteriormost suture between interparietal and occipital bone	medial
LIO	lateral interparietal occipital bone	lateral
SQ	posteriormost part of the zygomatic arch of the squamosal bone	lateral
O	posteriormost part of occipital bone	medial
Ventral side		
PM	most medial part of the suture between premaxilla and maxilla	lateral
PPF	anterior suture between premaxilla and maxilla on the palatine process	medial
PPP	posterior suture between maxilla and palatine process	medial
M1	anteriormost part of first molar	lateral
M3	posteriormost part of the third molar	lateral
ABT	anteriormost part of the tympanic bull	lateral
IF	posteriormost part of the incisive foramen	lateral
PF	posterior palatine foramen	lateral
PP	posterior palatine pit	medial
LPP	most lateral part of the junction between palatine and pterygoid process	lateral
AFM	anteriormost point of the foramen magnum	medial
PFM	posterior most point of the foramen magnum	medial

asymmetry. Signed asymmetry includes information about the direction of the asymmetry and is a measure for directional asymmetry. Signed asymmetry is then computed as the difference between the original and reflected copy. Unsigned asymmetry represents the magnitude of the difference between sides (right vs. left) but not the direction. The mean level of unsigned asymmetry in the population defined fluctuating asymmetry (FA) that is a measure of the developmental stability (Palmer and Strobeck 1986). Unsigned asymmetry is computed as the absolute value between the original and the reflected copy. Signed and unsigned asymmetries were corrected for the average of the directional asymmetry following the procedure described previously (Klingenberg et al. 2001).

STATISTICAL ANALYSIS OF SHAPE

Centroid sizes (dorsal and ventral side) of the superimposed configurations in the tangent space of every strain were compared to B6 using a Student's *t*-test and were submitted to the Bonferroni procedure.

Measurement error and quantification for variation were assessed with a Procrustes analysis of variance (ANOVA) adapted for object symmetry method (Klingenberg and McIntyre 1998; Klingenberg et al. 2002). In these ANOVAs, the main effect of individuals and strains stand, respectively, for individual and strain variation for shape. The main effect of reflection indicates directional asymmetry, whereas the reflection $\times$ individual interactions provides a measure of FA. Then, the residual variance among variance components quantifies measurement error. We conducted parametric tests on each effect with appropriate degrees of freedom as described by Klingenberg et al. (2002). To assess the pattern of variation of the skull shape, we carried out an analysis of the variance components for each landmark by the decomposition of the Procrustes mean squares for each effect of the both sides in the three-way ANOVA (Klingenberg and McIntyre 1998). Thus we summed x, y, and z mean squares of every landmark separately and computed the variance components according to the expected mean squares (Palmer and Strobeck 1986; Sokal and Rohlf 1995).

Shape is inherently multidimensional. Procrustes superimposition procedures in three dimensions eliminate seven degrees of freedom (reflection, translation, reduction and rotation). The relatively small sample size by strains and the large number of variables (respectively 66 and 57 Procrustes coordinates, 22 and 19 landmarks, on the dorsal and the ventral side corresponding to the x, y and z coordinates) could adversely affect the stability of the statistical analysis. To solve this problem, we performed a principal component analysis (PCA) on the covariance matrix of the tangent coordinates to reduce the number of variables according to the procedure previously described (Monti et al. 2001; Friess and Baylac 2003). We retained 20 principal components (PCs) and in all cases, these axes accounted for more than 96% of the total variance. We applied this methodology for all the analyses except for the Procrustes ANOVA. To identify significant QTL for shape and asymmetry on both sides, we conducted multivariate statistical tests between each IRCS and B6 as the reference group. A multivariate analysis of variance (MANOVA) was calculated on the shape coordinates (represented by the first 20 PCs of the reduced variables) with the strain effect as the main effect on the predicted values. Every MANOVA was submitted to a Bonferroni correction. Mean shape deformations were visualized by calculating the mean tangent coordinates of each group (the significant IRCS and B6) on the symmetric and the asymmetric component. To assess the amount of FA between an IRCS and B6, we conducted an extension of the Levene's test as previously described (Breuker et al. 2006). After Procrustes superimposition and the extraction of the signed asymmetry component as described previously, we followed the procedure described by Klingenberg and Monteiro (2005). A PCA was conducted on the corrected asymmetric coordinates and we scaled the first 20 PCs to obtain a variance equal to one. Procrustes and Mahalanobis distances were calculated on those reduced data to each individual with the average of B6 individuals as a reference. Thus, we conducted an ANOVA between every IRCSs and B6 with the Mahalanobis and the Procrustes distances as independent variables and the strains as a dependent variable and submitted to a Bonferroni method.

To investigate the relation between the length of SEG segments or the number of genes and the QTL effects, we conducted correlation tests between SEG fragment length or the number of genes encompassing the physical intervals for every strain (determined by the Mouse Genome Informatics website: http://www.informatics.jax.org/genes.shtml; Table 1) and QTLs effects size measured by the Procrustes distances. Therefore, the Procrustes distances were either the measure between every individual and the consensus individual or between every individual and the B6 as the reference (computed as the Procrustes distances between every individuals and the average of B6 individuals). These tests were carried out on the dorsal and ventral side of the skull, on the anterior part (maxilla and palatine bones, landmarks PPF, PPP, PM, IF, M1, PE), and the posterior part of the ventral side (most posterior part of the mid cranial fossa, temporal, and occipital bones, landmarks PP, AFM, PFM, M3, LPP, and ABT). All tests were carried out, for statistical significance, with 1000 permutations.

We also analyzed an IRCS 66H that showed strong differences in skull shape morphology with C57BL/6 mice. We performed a canonical variate analysis (CVA) based on 20 PCs separately on the ventral and dorsal side. A multivariate regression between a CVA axis and Procrustes coordinate in a tangent space was performed to visualize shape changes into a CVA axis. Classification rates were calculated by the leave-one-out cross-validation procedure (Lachenbruch and Michey 1968) of the R lda function. Generalized Mahalanobis distances (D^2) between groups were estimated on discriminant function. Groups were compared with Hotelling's T^2 test (Rao and Suryawanshi 1998). T^2 statistics follows an F distribution with t and $n1 + n2 - t - 1$ degrees of freedom, where t is the total number of groups, and $n1$ and $n2$, the number of individuals in the two groups under comparison. P-values were submitted to the Bonferroni correction. The power of the Hotelling's T^2-test was calculated as described in (Kelsey et al. 1996) when P was in the 0.05 to 0.1 range. Genetics determinism for FA was also assessed on 66H strain following the recommendations described in the previous section.

COVARIATION BETWEEN THE DORSAL AND THE VENTRAL SIDE OF THE SKULL

We analyzed the covariation between the dorsal and the ventral side of the skull. The degree of association between these two sides of the skull was determined by the two-blocks partial least-squares analysis (2B-PLS) (Rohlf and Corti 2000; Bookstein et al. 2003). This technique models the covariation between the two sets of variables being studied as a product of linear combinations of each of the sets. The linear combinations are computed by using a singular-value decomposition of the matrix of covariance between the dorsal and the ventral shape variables. The singular vectors are constructed in the form of new, paired latent variables (one per block) (Rohlf and Corti 2000) that accounted for as much as possible of the covariation between the two original sets of variables. To quantify the degree of morphological integration between two blocks of variables (e.g., the dorsal and the ventral side of the skull), we conducted an analysis of the correlation coefficient between the first PLS scores of those blocks as described by Rohlf and Corti (2000), Bookstein et al. (2003), and applied by Bastir and Rosas (2005), Gunz and Harvati (2007), Mitteroecker and Bookstein (2007)). The amount of covariance explained by the paired singular vectors, the correlation of the PLS scores along the singular axes of the two blocks, and 1000 permutations tests allowed statistical assessment of the observed singular values and correlations (Bookstein et al. 2003). A multivariate regression

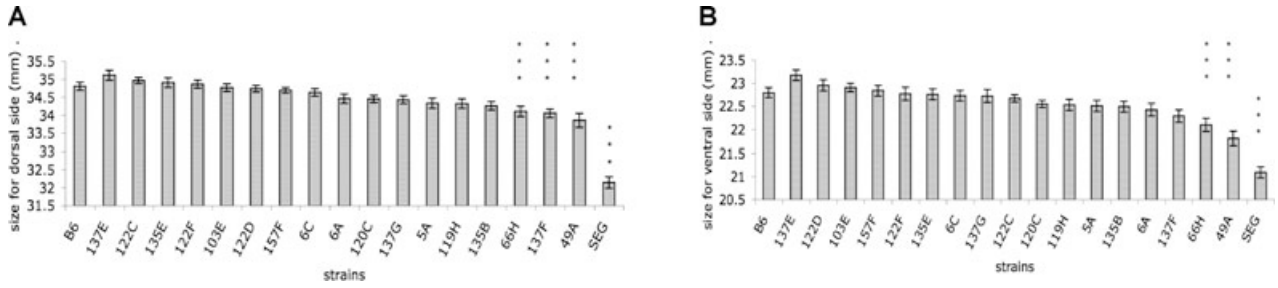

Figure 2. **Variations of size of IRCS skulls comparing to C57BL/6 and SEG/Pas on (A) Dorsal side, (B) ventral side. Centroid sizes were obtained after Procrustes superposition of all strains. Error bars show SEM. *** represented significant difference with C57BL/6 for $P < 0.05$ supporting Bonferroni method on the dorsal side (A) and the ventral side (B).**

between a PLS axis and Procrustes coordinate in a tangent space were conducted to visualize shape changes into a PLS axis.

All the statistical analysis was carried out with the pre released of Rmorph library (Michel Baylac baylac@mnhn.fr) on R version 2.7.0 (http://www.r-project.org) and additional programming were performed with MASS library (Gaétan Burgio).

Results

ANALYSIS FOR CENTROID SIZE

The centroid size of the skull differed significantly between the parental strains SEG/Pas (32.16 ± 0.16 mm on the dorsal side and 21.08 ± 0.12 mm on the ventral side) and B6 (34.79 ± 0.11 mm and 22.11 ± 0.12 mm, respectively, with $P < 0.0001$ for both sides) (Fig. 2A,B). Most notable were the IRCS 49A (32.85 ± 0.19 mm and 21.08 ± 0.16 mm, respectively) and 66H strain (34.1 ± 0.14 mm and 22.1 ± 0.14 mm, respectively), which were significantly smaller than B6 strain on both sides ($P < 0.0001$). On the dorsal side, 137F strain was smaller than B6 (34.04 ± 0.11 mm, $P < 0.0001$). The analysis of the different allelic combinations of 66H showed that little size was shared by the chromosome 1 SEG allele (34.07 ± 0.11 mm and 22.03 ± 0.11 mm, respectively, with $P < 0.0001$) and the addition of the chromosome 18 and the chromosome 1: (66H-Chr1+18) on the ventral side (22.26 ± 0.12 mm, $P = 0.02$).

SOURCE OF VARIATION IN SHAPE

Procrustes ANOVA provides a measure of the amount of measurement error and asymmetry. Table 3 shows the results of the Procrustes ANOVA. Mean square for side is a measure for directional asymmetry and reflection × individual interactions is a measure for FA. Variation among strains clearly contributed a very high amount of the total shape variation on both sides (70.2% on the dorsal side and 86.2% on the ventral side). Variation among individuals accounted for less than 15% of the total variation (14.6% and 7.8%, respectively). Directional asymmetry was also significant but to an even lesser extent (1.41% dorsal, 0.75% ventral). The variance components representing FA were higher than

Table 3. **Procrustes ANOVA on the dorsal and ventral sides of the skull. Procrustes ANOVA of the amounts of shape variation attributable to different sources. Sum of squares, mean squares, and variance components are in units of squared Procrustes distance (variance components × 10^6. The percentage contributions (% variance) of each variance component to the total variance also are given. ***indicate $P<0.01$**

	Sum of squares	df	Mean square	Variance components	% variance
Dorsal side					
Individuals (I)	2.6464	9440	0.0002***	35.7	14.6
Reflection (R)	0.1654	27	0.0061***	3.5	1.41
I×R	0.5232	7965	6.5×10^{-5}***	31.9	13
Strains (S)	0.8898	704	0.00126***	171.97	70.2
Error	0.0307	17464	1.7×10^{-6}	1.75	0.7
Ventral side					
Individuals (I)	3.0266	7965	0.000379***	53.1	7.8
Reflection (R)	0.2067	23	0.00898***	5.05	0.75
I×R	0.4481	7080	6.32×10^{-5}***	28.17	4.18
Strains (S)	2.0700	594	0.00384***	547.41	86.2
Error	0.1027	14800	6.93×10^{-6}	6.93	1.02

Table 4. Variance components for the effects in the Procrustes ANOVA listed by landmark by sides; 14 landmarks on the dorsal side and 12 landmarks on the ventral side. All entries have been multiplied by 10^8 to make them more readable.

	Effect				
Landmark	Individuals	Reflection	Individuals × Reflection	Strains	Error
Dorsal side					
ANB	83	3	52	458	8
IN	68	3	22	280	6
FP	173	0	95	1335	5
PI	79	2	130	425	0
IO	224	1	96	1582	1
O	249	7	60	929	3
NPM	60	8	99	514	8
PMM	29	41	298	351	36
FN	398	5	65	684	9
MF	443	4	55	1650	20
LFP	50	8	90	342	1
LIO	44	79	307	387	3
MZ	248	8	223	2760	1
SQ	74	7	232	428	8
Ventral side					
PPF	237	14	43	1338	6
PPP	355	0	7	3717	29
PP	501	5	47	5616	52
AFM	146	62	128	454	14
PFM	264	10	75	1842	197
PM	31	33	644	179	63
M1	54	20	69	500	1
IF	175	3	61	1852	4
PE	111	2	91	1092	2
M3	799	25	63	8939	76
LPP	432	33	113	4851	14
ABT	348	90	229	3378	15

the corresponding directional asymmetry for both sides among individuals (13% dorsal, 4.18% ventral). The mean square for FA and individual and strain variation exceeded error components. Significance testing for directional and FA indicated that measurement error was negligible compared to the biological-shape variation.

QUANTIFICATION OF VARIATION IN SHAPE

The Procrustes ANOVA for shape variation showed that all effects of the model were statistically significant (Table 3). Therefore, we examined the pattern of shape variation by landmarks and by effects (Table 4). On the dorsal side, variation among strain and individual were highly significant and affected landmarks FP, IO, O, MF, and MZ. These landmarks were located both on the top of the cranial vault, on the cranial suture between the maxilla and the frontal bone, and on the anterior part of the zygomatic bone. For the directional asymmetry effect, the largest left–right effect was found on the lateral side of the skull (PMM and LIO). Landmarks located on the most lateral side of the skull (the zygomatic bone MZ and SQ, the face PMM, and the temporo–parieto–occipital suture LIO) caused most of the effects for FA. On the ventral side, individual and strain effects were highly significant and affected the posterior part of the ventral side (basioccipital, PP and ABT; the temporal bone, LPP; and posterior part of the maxilla, PP and M3). In contrast, landmarks located on the anterior cranial fossa (PPF, AFM, and M1) varied little between effects for individual and strain effects. For FA, landmarks on the lateral side of the basioccipital (LPP and ABT) and notably on the maxilla (PM) varied greatly. Overall, the majority of the quantity of the variation on the dorsal side was located on the cranial vault for individual and strains effect and on the most lateral side of the skull for FA effects. On the ventral side, the posterior regions including the midcranial fossa, the temporal, and the occipital represented a large amount of the variation for the individual and strain effects. The maxilla had the highest contribution of the variation of FA.

QTLS FOR SHAPE AND ASYMMETRY

QTLs associated with dorsal and ventral skull shape were identified using MANOVAs on the 20 first principal components on each IRCSs. Significant QTLs were found, for all the strains except 135E (a monocongenic strain with a SEG segment mapped on the chromosome 19 telomere). On the dorsal side, spatial patterning of significant IRCSs on the MANOVAs tests affected all the landmarks (49A, 120C, 122C, 122D, 137G, and SEG) (Fig. S1). We found QTLs that affected the zygomatic arch (landmarks MZ and SQ) by elevating (6C, 49A, 119H, 137E, 137F, and 157F) or lowering (103E and 120C) its position. Similarly, QTLs associated with elevating (103E, 119H, 122D, 135B, and 137G) or lowering (6A, 49A, 137F, and 157F) of the cranial vault (landmarks PI, IO, and O) were found. A relative shift in opposite direction between the landmarks IO and LIO on the antero–posterior and the supero-inferior axis were also observed, corresponding to a shortening of the cranial vault (6A, 66H, and 137F) or a lengthening and enlarging of the parietal bone (103E, 119H, 120C, 122F, 137E, and 157F). In contrast, except for the strains 49A, 66H, 122C, 135B, and 137G, the shape changes for the landmarks located on the face were slight. On the ventral side, spatial patterning is shown in Figure S2. Most of shape changes occurred on the temporal and the basioccipital bone (landmarks AFM, PFM, LPP, and ABT) either by a lengthening (strains 6A, 6C, 49A, 103E, 122C, 135B, and 137E) or a shortening (5A, 119H, and 122D). In addition, enlargement in the antero–posterior axis of the maxilla and palatine bones (landmarks M1 and M3) was observed in the strains 5A, 119H, 122D, 137E, and 157F. Moreover, the shape changes on the maxilla bone were subtle and mostly affected the landmark PM by a shortening (strain 6A, 49A, 66H, 137G) or an elevation (119H or 122D). Analysis of the amount of the FA with the IRCSs revealed nonsignificant effects on the variation of FA on the dorsal side either with SEG ($F_{[17,360]} = 1.6$, $P = 0.057$ on Procrustes distances and $F_{[17,360]} = 1.55$, $P = 0.07$ on Mahalanobis distances) or without SEG ($F_{[17,360]} = 0.91$, $P = 0.55$ and $F_{[17,360]} = 0.95$, $P = 0.5$, respectively) while the amount of FA was significant on the ventral side either with SEG ($F_{[17,360]} = 5.9$, $P < 0.0001$ on Procrustes distances and $F_{[17,360]} = 6.32$, $P < 0.001$ on Mahalanobis distances) or without SEG ($F_{[17,360]} = 2.36$, $P = 0.0018$ and $F_{[17,360]} = 2.37$, $P = 0.0018$, respectively). Additionally, exploration of the SEG segment effects on the IRCSs did not show a significant effect. Only one QTL affected FA on the dorsal side (strain 120C) and the ventral side (strain 66H) (Table 5). However, ANOVAs did not confirm those finding on 120C strain ($F_{[1,41]} = 5.3$, $P = 0.36$ on Procrustes distances and $F_{[1,41]} = 3.8$, $P = 0.8$ on Mahalanobis distances) and on 66H strain ($F_{[1,42]} = 6.13$, $P = 0.3$ on Procrustes distances and $F_{[1,42]} = 5.07$, $P = 0.5$ on Mahalanobis distances) whereas significant effect of SEG on FA was found only on the ventral side ($F_{[1,31]} = 25$, $P < 0.0001$ on Procrustes distances and $F_{[1,31]} = 15.81$, $P < 0.0001$ on Mahalanobis distances). On the dorsal side the quantitative trait of 120C affected mostly the top of the cranial vault on the lateral axis (landmarks PI and IO), the zygomatic arch (landmarks MZ and SQ) on the postero–inferior and the antero–posterior axes and the squamoso-parietal suture (landmark LIO) on the lateral and the supero–inferior axes (Fig. 3). On the ventral side, landmarks located on the maxilla and the palatine (PPP, M1, IF, and M3) bones were likely affected on the lateral axis (Fig. 3). No QTLs associated with directional asymmetry were found whereas the analysis of the Procrustes ANOVA was significant.

CORRELATION BETWEEN SEG GENOME LENGTH AND PROCRUSTES DISTANCES

We investigated the correlation between skull shape modification and SEG DNA fragment length as a surrogate for the number of genes that may be contributing to significantly associated features. On the dorsal side, correlations between SEG genome length or the number of genes and dorsal Procrustes distances were significant, either with the consensus individual ($r = 0.52$, $P = 0.012$ on SEG segment length, [Fig. 4A] and $r = 0.61$, $P = 0.007$ by the number of genes) or based on B6 strains ($r = 0.57$, $P = 0.004$ and $r = 0.37$, $P = 0.05$, respectively). On the ventral side, we observed no correlations between SEG genome length and either the consensus individual ($r = 0.24$, $P = 0.29$ [Fig. 4B] and $r = 0.07$, $P = 0.39$, respectively) or B6 based ($r = 0.29$, $r = 0.118$, and $r = 0.34$, $P = 0{,}074$ respectively). After removing four strains (49A, 120C, 135E, and 137E), we identified a significant correlation with SEG segment length ($r = 0.45$, $P = 0.04$ on the consensus individual and $r = 0.44$, $P = 0.04$ with B6 as a reference), but not with the number of genes ($r = 0.16$, $P = 0.28$ and $r = 0.22$, $P = 0.21$, respectively). The magnitude of the Procrustes distances between the IRCSs and the shape consensus was low (0.235 to 0.240) but the average was high and equal to 0.236. In contrast, center to B6, the magnitude was 0.015 and the average was equal to 0.033. To verify the assumption of the discrepancy of QTLs effects on both sides, we carried out a complementary analysis on the basicranium and on the anterior part of the ventral side (Fig. 4C,D). It confirmed a significant relationship between Procrustes distances and SEG length fragments or the number of genes on the basicranium and the midcranial fossa (consensus reference: $r = 0.52$, $P = 0.004$ with SEG segment length and $r = 0.41$, $P = 0.038$ by number of genes, with B6 as a reference: $r = 0.48$, $P = 0.02$ and $r = 0.415$, $P = 0.046$, respectively) and a nonsignificant relationship between Procrustes distances and SEG length fragments ($r = 0.03$, $P = 0.41$ and $r = 0.12$ $P = 0.284$, respectively) or the number of genes ($r = 0.101$ $P = 0.33$ and $r = 0.108$, $P = 0.33$) on the anterior part of the ventral side.

Table 5. MANOVA analysis on the ventral and dorsal side shape and unsigned asymmetry. MANOVA tests for differences in shape and asymmetry by testing between group, i.e., an IRCS with C57BL/6, strain as the main effect. Shape is described as the 20 first principal components of the tangent coordinates in the shape space. Unsigned asymmetry is described as the 20 first principal components of the absolute difference between tangent coordinates of the nonreflected and reflected shape. *P* values are corrected after Bonferroni adjustment.

	Dorsal side Group					Ventral side Group					
	Wilks	*F*	*P* value	df num	df den		Wilks	*F*	*P* value	df num	df dem
Shape											
66H	0.1305	7.664	<0.0001	20	42	66H	0.1257	8	<0.0001	20	42
5A	0.212	3.903	0.0270	20	40	5A	0.1609	5.4766	0.0025	20	40
6C	0.1309	8.6302	<0.0001	20	45	6C	0.1361	8.2526	<0.0001	20	45
103E	0.0576	10.6433	<0.0001	20	32	103E	0.0806	7.412	0.0055	20	32
119H	0.1851	4.8441	0.0048	20	41	119H	0.1631	5.6451	0.0015	20	41
120C	0.0446	23.5675	<0.0001	20	41	120C	0.052	20.041	<0.0001	20	41
122C	0.0627	14.9465	<0.0001	20	39	122C	0.0719	12.9152	<0.0001	20	39
122D	0.0806	9.1202	0.0274	20	35	122D	0.1	7.1962	0.0019	20	35
122F	0.1336	4.8636	0.0004	20	34	122F	0.1285	5.087	0.0214	20	34
135B	0.0484	18.6924	<0.0001	20	38	135B	0.035	26.23	<0.0001	20	38
135E	0.2829	2.407	n.s.	20	38	135E	0.2551	2.774	n.s	20	38
137E	0.1515	4.7	0.0180	20	36	137E	0.1223	6.0986	0.0038	20	36
137F	0.15	4.8172	0.0170	20	36	137F	0.1082	7	0.0015	20	36
137G	0.1167	7.1898	<0.0001	20	38	137G	0.1197	6.985	0.0007	20	38
157F	0.0771	7.7775	0.0043	20	32	157F	0.1034	5.6392	0.0230	20	32
6A	0.0695	11.3734	<0.0001	20	36	6A	0.0728	10.825	<0.0001	20	36
49A	0.0362	17.3237	<0.0001	20	32	49A	0.0466	13.3	<0.0001	20	32
SEG	0.0318	18.296	<0.0001	10	31	SEG	0.014	40.872	<0.0001	20	31
Unsigned asymmetry											
120C	0.1872	3.948	0.027	20	41	66H	0.295	3.65	0.025	20	42

THE GENETIC ARCHITECTURE OF SHAPE VARIATION IN 66H STRAIN

We focused our study on the 66H strain, which had a significant effect on our precedent analyses (Fig. 5). We carried out a CVA on all 66H allelic combinations, based on the first 20 PCs. The total classification rate was 64.38% on the dorsal side. On the dorsal side, all the allelic combinations except the strain 66H-Chr13 ($T^2 = 6.22$, $F_{[8,44]} = 7.27$, $P = 0.14$) exhibited significant differences with C57BL/6 (data not shown). The examination of the bicongenic strains showed different epistatic effects of 66H alleles. To compare between the various 66H congenic strains, statistical inference using Hottelling tests was applied on Mahalanobis distances. 66H-Chr13+18 differed significantly from 66H-Chr13; but not from 66H-Chr18 while 66H-Chr1+13 differed significantly from 66H-Chr1 but not from 66H-Chr13. Therefore, 66H-Chr1+18 contrasted significantly with 66H-Chr1 and did not significantly vary from 66H-Chr18 (Table 6). Shape changes were studied using a multivariate regression along the

Table 6. Tests of hypotheses of 66H strain allelic combinations based on Hotelling's generalized T^2 statistics.

	Dorsal side				Ventral side					
	T^2	*F*	*P* value	Statistical power (1−ß)	T^2	*F*	*P* value	Statistical power (1−ß)	df num	df dem
66H-Chr13+18 vs 66H-Chr13	20.78	28.17	0.0017		7.83	9.45	0.0630	0.63	8	55
66H-Chr13+18 vs 66H-Chr18	7.85	9.48	0.0620	0.61	6.59	7.81	0.1100		8	57
66H-Chr1+13 vs 66H-Chr1	8.95	10.95	0.0390		4.1	4.61	0.5600		8	53
66H-Chr1+13 vs 66H-Chr13	7.44	8.91	0.0760	0.62	9.05	11.09	0.0370		8	53
66H-Chr1+18 vs 66H-Chr1	19.91	26.71	0.0020		8.14	9.48	0.0560	0.81	8	47
66H-Chr1+18 vs 66H-Chr18	7.96	9.59	0.0610	0.76	11.15	13.96	0.0180		8	49

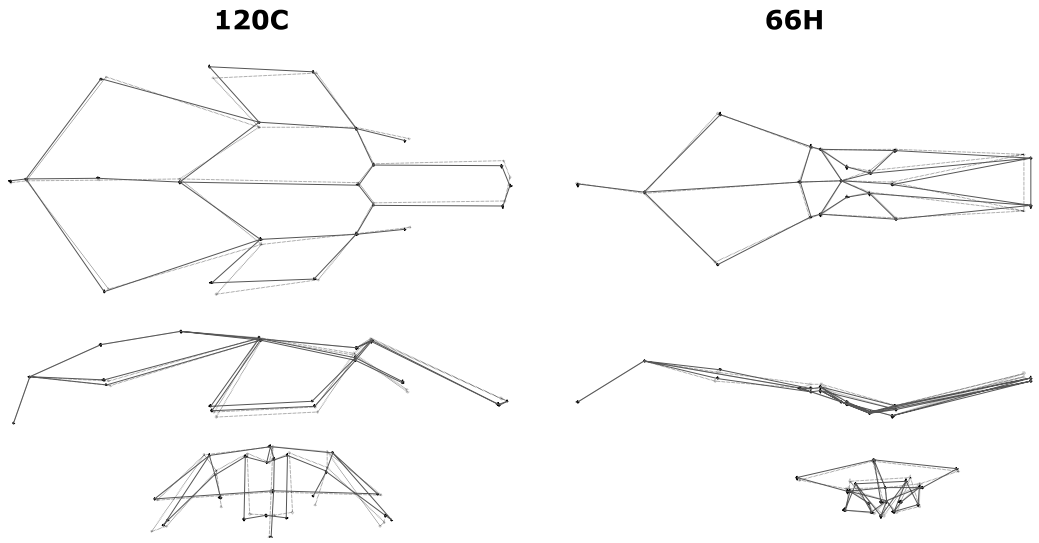

Figure 3. **Visualization of unsigned asymmetry on the dorsal and ventral side. For each strain exhibited a significant difference with C57BL/6 on the MANOVA test after Bonferroni correction, the modification for shape is shown. In each diagram, the landmarks are indicated by the dots and the solid lines represented the mean shape for C57BL/6 whereas the dashed lines represented the mean shape for the IRCS strain. Because the QTL effects are subtle for FA, the shapes changes have been amplified by 7 on the dorsal side and by 4 on the ventral side.**

first and second canonical axes. Only a minor shape change on the cranial vault (landmarks FP and IO) and the zygomatic arches (landmark SQ) was observed on the first canonical axis (Fig. 5). Shape changes on the second canonical axis were characterized by a lengthening on the lateral axis and an elevation (landmarks IO, FP, and LIO) of the cranial vault, an elevation or a lowering of the nasal bone shape (landmarks ANB and NPM), and an obtuse or an acute angle between the zygomatic arches and the superior maxilla (landmarks MZ and MF). Analysis of FA on 66H strain by MANOVAs tests on the first 20 PCs, showed a significant differences between 66H-Chr18 and B6, (Wilks $\lambda = 0.36$, $F_{[20,37]} = 2.66$, $P = 0.04$) but no significant variation with the other substrains. Complementary analysis of the bicongenic strains with 66H-Chr18 showed significant differences with 66H-Chr13+18 (Wilks $\lambda = 0.47$, $F_{[20,40]} = 2.38$, $P = 0.046$), and 66H-Chr13 (Wilks $\lambda = 0.36$, $F_{[20,49]} = 3.75$, $P < 0.001$), but no significant

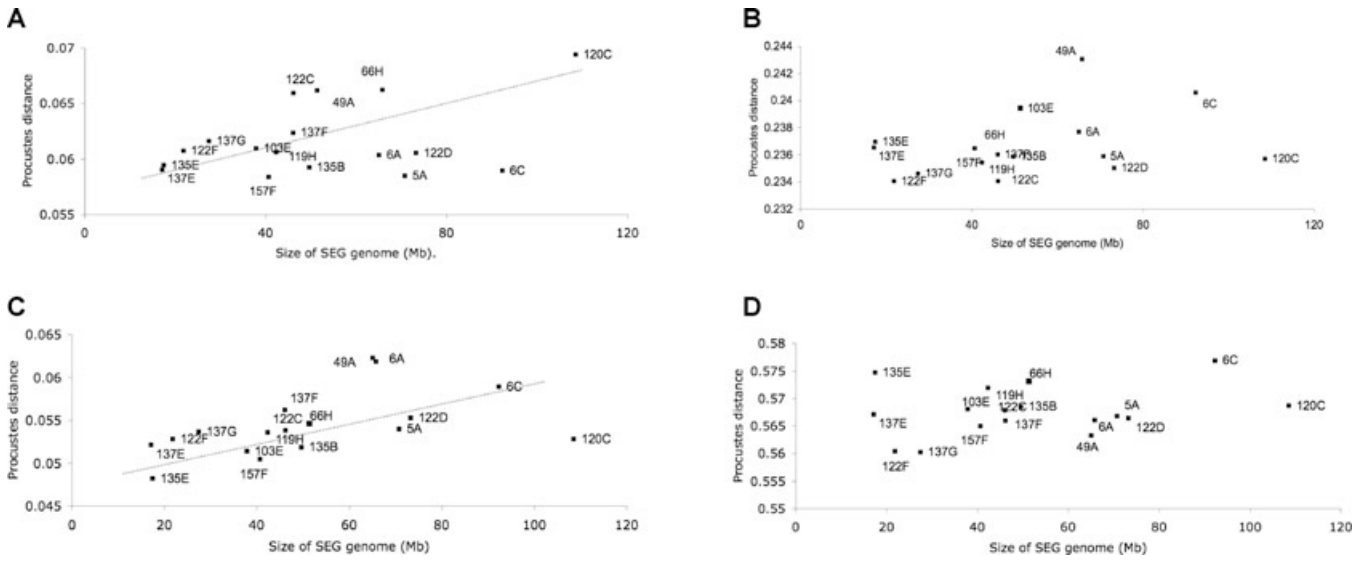

Figure 4. **Relation between Procrustes distances between the consensus shape and IRCS strains and length of SEG/Pas segments on (A) dorsal side, (B) ventral side, (C) the basicranium and (D) the anterior and middle cranial fossa of the ventral side. The x-axis represented the size of SEG genome per strains in megabases and the y-axis, the Procrustes distances in millimetres. The dashed line indicated the significant correlation between the Procrustes distances and length of SEG/Pas segments.**

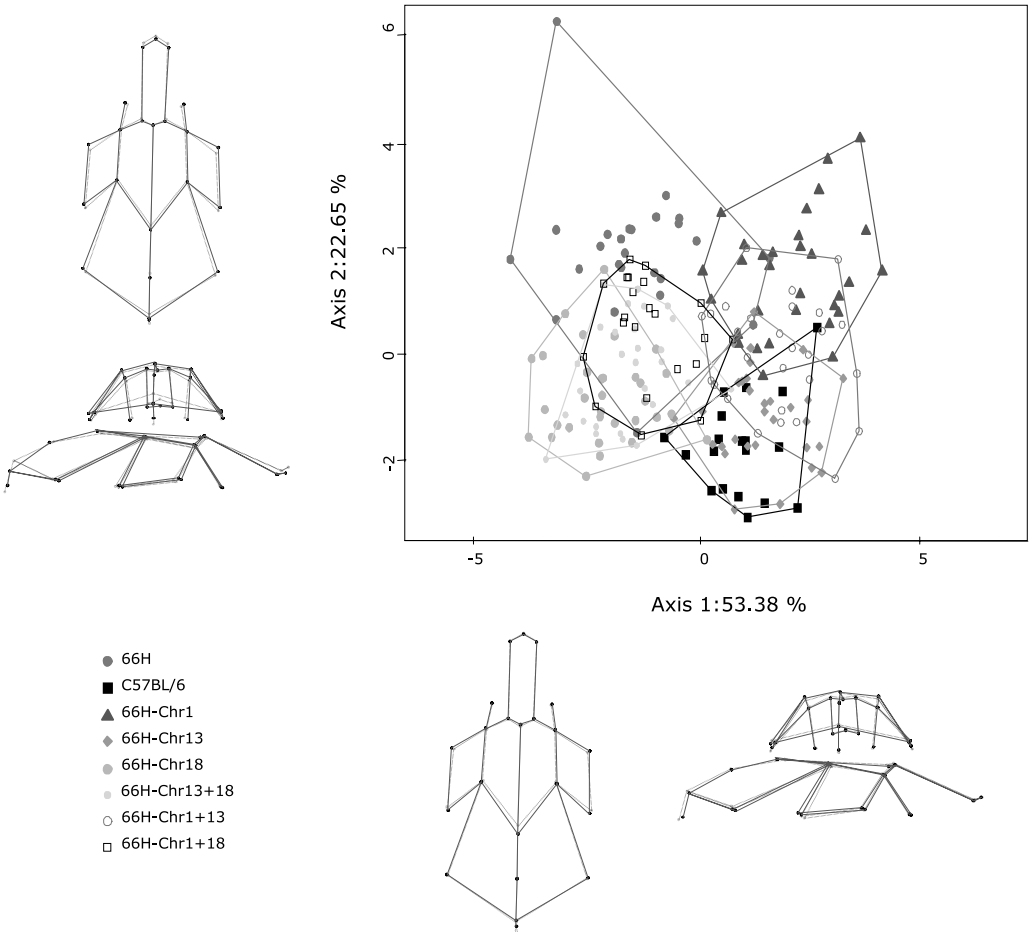

Figure 5. Comparison on dorsal shape in all allelic combinations of the strain 66H, 66H, and C57BL/6, by CVA based on 20 principal Components axes after Procrustes superimposition. The first and the second canonical axes were represented, totaling 77%. Shape drawn outside of the scatter plot, calculated with a multivariate regression, described dorsal shape variation along the canonical axes with low values (dashed lines) and high values (solid lines). No amplification of the shape changes was effected.

variation with 66H-Chr1+18 Wilks $\lambda = 0.4$, $F_{[20,48]} = 2.1$, $P = 0.09$). Visualization of shape changes (Fig. S3) showed a modification of shape in all landmarks with a shortening of the face, a shift between the landmarks MZ, SQ, LFP, and LIO on the right and left side (lateral axis), and a left shift of the landmarks IN, IO, and O on the cranial vault. However, ANOVAs did not confirm these findings for the 66H-Chr18 strain ($F_{[1,50]} = 0.03$, $P = 0.9$ on Procrustes distances and $F_{[1,50]} = 0.06$, $P = 0.94$ on Mahalanobis distances).

On the ventral side, the total classification rate was 58% (Fig. 6). A large overlap between strains was observed. However, all the strains showed significantly differences with B6 shape at $P < 0.05$ after the Bonferroni correction (data not shown). We also observed different epistatic effects of 66H alleles with the examination of the bicongenic strains. Statistical inference using Hottelling test on Mahalanobis distance confirmed that B6-Chr13+18 did not differ significantly from 66H-Chr18 or 66H-Chr13. 66H-Chr1+13 varied significantly from 66H-Chr13 but not from 66H-Chr1 while 66H-Chr1+18 was significantly different from 66H-Chr18 but not from 66H-Chr1 (Table 6). Visualization of shape changes highlighted minor differences on the lengthening of the basicranium (landmarks PP and ABT) along the antero–posterior and lateral direction along the first canonical axis, and a lengthening on the basicranium (lateral direction) and the anterior cranial fossa (landmarks ABT, LPP, M3, and M1) on the second canonical axis. Analysis of FA on the 66H strain by a MANOVA on the first 20 PC's showed significant differences between 66H-Chr18 and B6, (Wilks $\lambda = 0.41$, $F_{[20,37]} = 2.82$, $P = 0.033$ after Bonferroni correction). Complementary analysis using allelic combinations involving 66H-Chr18 showed significant differences to 66H-Chr1+18 (Wilks $\lambda = 0.39$, $F_{[20,53]} = 2.6$, $P = 0.035$) and 66H-Chr13 (Wilks $\lambda = 0.44$, $F_{[20,49]} = 2.73$, $P = 0.01$), but not to 66H-Chr13+18 (Wilks $\lambda = 0.52$, $F_{[20,48]} = 1.94$, $P = 0.17$). Visualization of shape changes (Fig. S3) showed minor modifications on the maxilla and a right displacement of the landmarks PP, AFM, and PFM. However, analysis of the amount of

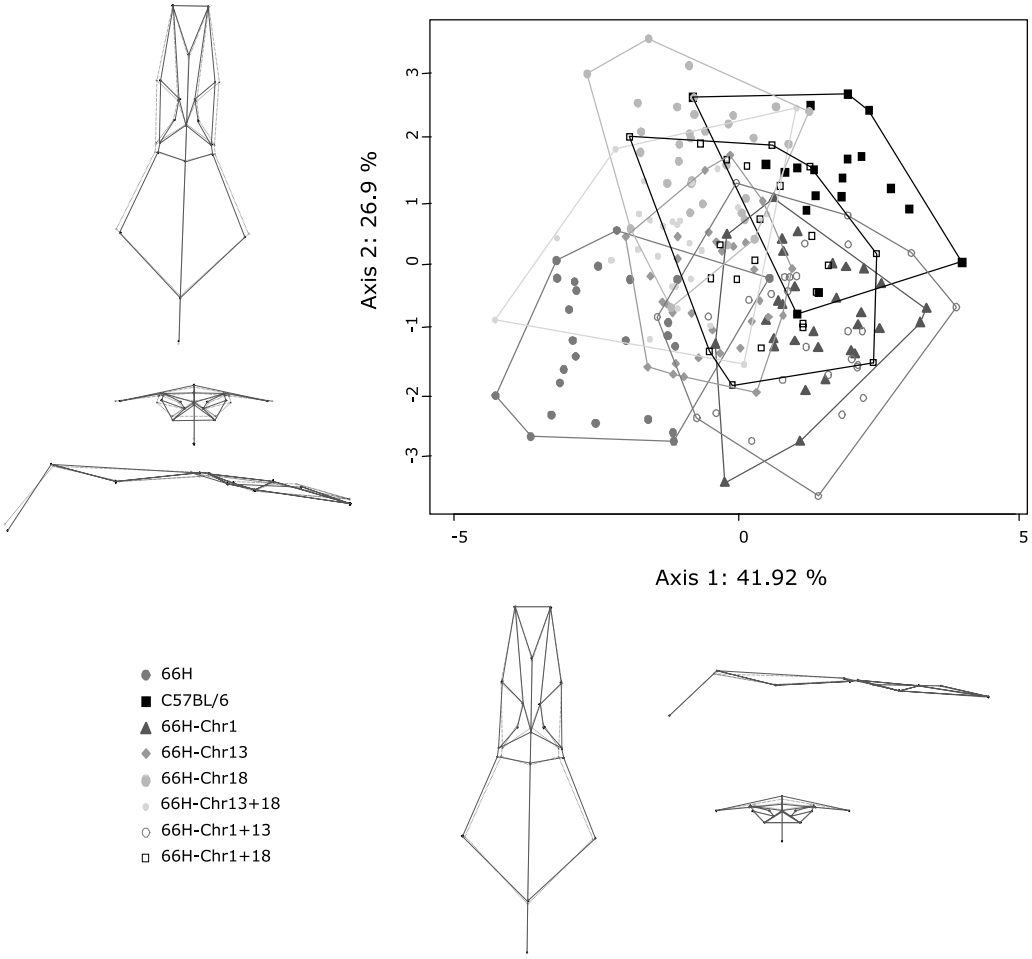

Figure 6. Comparison on ventral shape in all allelic combinations of the strain 66H, 66H, and C57BL/6, by canonical variate analysis based on 20 principal components axes after Procrustes superimposition. The first and the second canonical axes were represented, totaling 68.8%. For explanation of the diagrams, see Figure 5. Shape changes were amplified by a factor of 3.

FA did not confirm these previous findings on 66H-Chr18 strain ($F_{[1,50]} = 0.003$, $P = 0.95$ on Procrustes distances and $F_{[1,50]} = 0.06$, $P = 0.94$ on Mahalanobis distances). 66H-Chr18 significantly differed from 66H-Chr1+18 ($F_{[1,51]} = 18.5$, $P < 0.0001$ on Procrustes distances and $F_{[1,51]} = 16.48$, $P < 0.001$ on Mahalanobis distances) but not from 66H-Chr18 *Chr13+* ($F_{[1,61]} = 3.46$, $P = 0.3$ on Procrustes distances and $F_{[1,61]} = 3.14$, $P = 0.4$ on Mahalanobis distances).

PATTERN OF COVARIATION

Patterns of covariations between the dorsal and the ventral sides of the IRCSs were studied using the 2B-PLS method (Fig. 7A). Covariation between the two sides (accounting for 72% of total squared cross-covariance for all IRCSs) on the first PLS axis was strongly correlated (correlation on cross-covariance matrix was equal to 0.8, $P < 0.001$). The other 14 axes were also significantly correlated ($P < 0.001$), corresponding to 99.83% of the cumulated total squared cross-covariance (for more details, see Supporting Table S1). All the strains except 49A, 119H, and 6A were distributed upon a line extending from 137G to 120C. The SEG strain had negative coordinates for both axes (value was equal to –0.03 on both sides on the first PLS block, data not shown). The 120C and 66H strains exhibited small differences compared with B6. In contrast, 137G and 103E strains showed large differences to B6. Interestingly, the strains 49A and 119H were outliers on the 2B-PLS analysis and the modifications for shape occurred mostly on the dorsal side for 49A and on the ventral side for 119H in agreement with our previous analyses (Figs. S1 and S2). Test for correlation between the first PLS axis and SEG segment length or by number of genes was not significant (first PLS axis, dorsal side: $r = 0.35$, $P = 0.011$; first PLS axis, ventral side $r = 0.31$, $P = 0.08$; by the number of genes on the first PLS axis, dorsal side: $r = 0.11$, $P = 0.33$ and ventral side: $r = 0.17$, $P = 0.22$). Visualization of shape deformations was analyzed with a multivariate regression in the first PLS axis. Shape changes in the first axis were characterized by a change

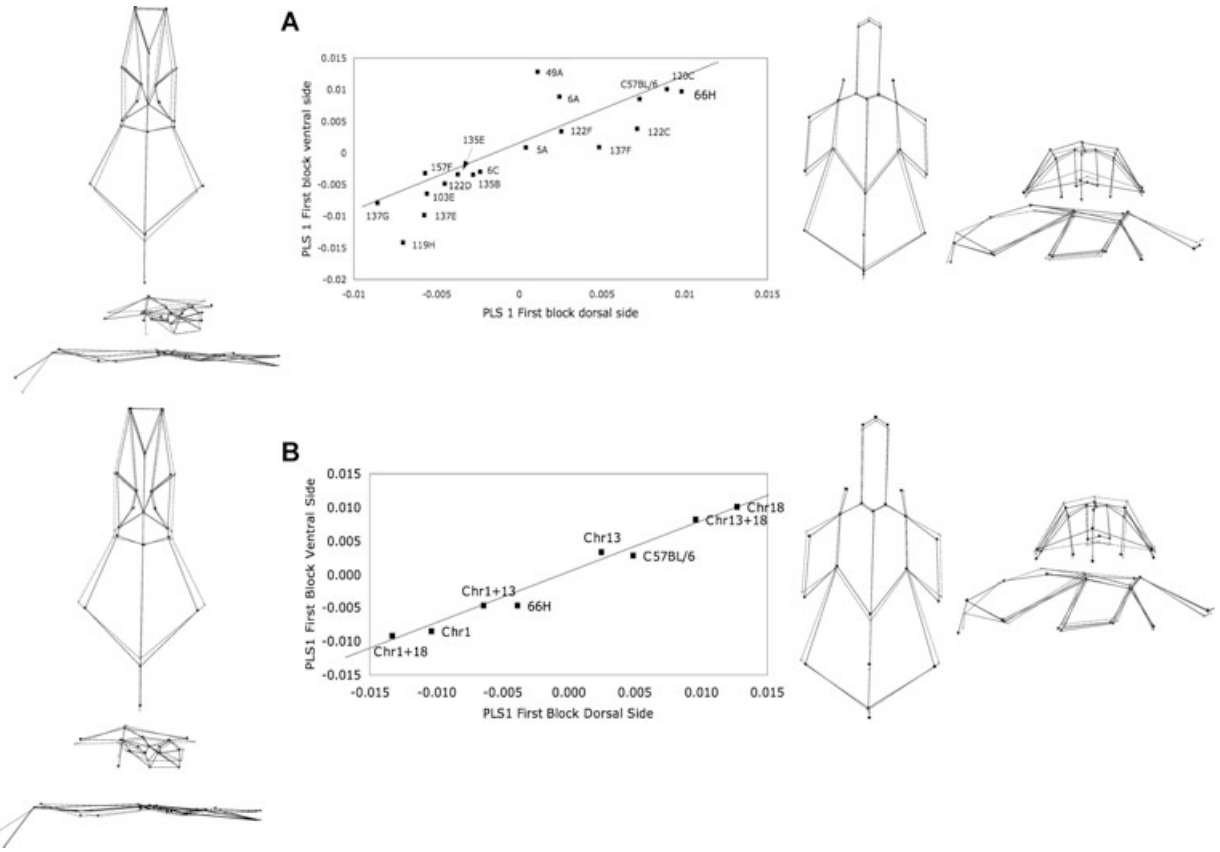

Figure 7. Covariation between dorsal and ventral side of IRCSs compared to C57BL/6 mice (A) and allelic combinations of 66H strains and C57BL/6 (B) with two-blocks partial least squares (2B-PLS). The graph represented the distribution of the strains along the first PLS axis corresponding to 87% of the explained cross-covariance. The correlation on covariance matrix is 0.8 ($P < 0.001$). The x-axis represented the dorsal side for first block and y-axis, the ventral side. Correlation between the 2-B-PLS was shown by a dashed line. Dorsal and ventral shape variations along the PLS axes with low values (dashed lines) and high values (solid lines) are shown outside of the graph. Chr1 for example was the abbreviation of 66H-Chr1.

in the lengthening on the lateral axis (landmark LIO), an elevation or lowering of the cranial vault (landmarks FP, IO), the nasal bone shape (landmarks ANB and NPM), or the zygomatic arches (landmarks MZ and SQ). On the ventral side, variability affected the lengthening in the lateral axis (landmarks ABT, M3, and M1) and occipital foramen elevation or lowering (landmark O).

Analysis of the pattern of covariation between the both sides for all allelic combinations of the 66H strain (Fig. 7B) showed a strong correlation of the first PLS axis ($r = 0.75$ with $P < 0.001$ corresponding to 86.86% of the total squared cross-covariance). The other 10 axes were also significantly correlated ($P < 0.001$) corresponding to 99.65% of total cross-covariance (for more details, see Supporting Table S1). All the 66H allele combinations of strain were distributed upon a line extending from 66H-Chr1+18 to 66H-Chr 18. The SEG strain was an outlier and negative for both axes (value is equal to –0.03 on both sides on the first PLS block, data not shown). We also separated the strains into two groups. The first one comprised the strains C57BL/6, B6-Chr13, 66H-Chr13+18, and 66H-Chr18. The second group contained the strains 66H, 66H-Chr1+13, 66H-Chr1+18, and 66H-Chr1. We observed an association between B6-Chr1 and 66H-Chr1+18 and between 66H-Chr18 and 66H-Chr13+18. 66H-Chr1+13 had an intermediate position between 66H-Chr1 and 66H-Chr13. Shape changes in the first axis were characterized by the same changes as previously described for IRCSs but in opposite direction.

Discussion

A LARGE NUMBER OF QTLS CONTROLLED SKULL SHAPE VARIATION

The combination of the genetic and phenotypic polymorphism of the wild-derived strains and morphometric geometrics methods led us to explore the genetic variation of skull shape and morphological integration. With 17 IRCSs covering 25% of SEG genome, we showed that nearly all the IRCSs (16/17 strains on both sides) exhibited a significant shape variation compared to C57BL/6 mice (Table 5). Even though the average segment length was large

(corresponding to 11 Mb and more than one QTL could be detected onto one fragment) and all the SEG genome was not covered (due to hybrid incompatibility and counter-selection of *Mus spretus* genome by C57BL/6), the introduction of few SEG-derived fragments into C57BL/6 genome induced significant changes on the skull shape (Table 5 and Figs. S1 and S2). Dissection of SEG allelic contribution of one IRCS, which resulted in reduced segment length and isolated still yielded in significant skull shape changes. The only previously published work that is comparable is the QTL mapping of the skull shape variation performed by Leamy et al. (1999). Most of the IRCSs (at least 12/17 strains on both sides) identified QTLs not previously reported. However, one QTL mapped in an equivalent region (QTL-S1.1 with 66H strain). Other potentially matching QTLs with the previous study were (QTL-S11.1 with 122D, QTL-S12.2 with 120C, QTL-S17.2 with 6C, QTL-S19.1 with 103E). But progeny testing of the IRCSs is required to confirm these. Spatial patterning of the shape variation, showed by the visualization of shape changes (Figs. S1 and S2) and analyzed by the variance components on the strain effect, also indicated a high contribution on the variation of the cranial vault (41% of the total variance), the zygomatic arches (26% of the total variance only with two landmarks) and the posterior cranial fossa (74% of the total variance). In contrast, a low variation in the spatial patterning was found on the face (26% of the total variance) and on the anterior cranial fossa (22% of the total variance). Analysis of effect sizes for the QTLs (using the Procrustes distances) between SEG segments, or by gene density showed a discrepancy between the ventral and the dorsal side. A lack of correlation between Procrustes distances and either SEG segment length or number of genes on the anterior part of the ventral side (Fig. 4D), contrary to the dorsal side and the basicranium (Fig. 4A,D) explained that discrepancy. Additionally, the Procrustes ANOVA and the variance component analyses confirmed the differential patterning. Moreover, positive and significant correlation between Procrustes distances and either SEG segments length or number of genes indicated an additive relationship between SEG segment length and Procrustes distances. This suggests a large number of QTLs may control variation on overall skull, with the exception of the anterior part of the ventral side. Since the SEG segments of all the IRCSs strains examined were homozygous (due to inbreeding over 20 generations), the role of dominance was not assessed.

QTL EFFECTS AND PLEIOTROPY

Detailed analysis of shape changes for all IRCSs indicated two different categories of pleotropic effects on the skull shape. Some strains (49A, 122C, or 137G) exhibited a modification of all landmarks on both sides (Figs. S1 and S2). The pleiotropic effect was on the overall skull shape and this variability could be linked to a major genetic effect of SEG segments. Several QTLs were also found to affect different bones simultaneously; mostly the cranial vault or the zygomatic bone, on the dorsal side or the basicranium on the ventral side (Table 4). Visualization of shape changes (Figs. S1 and S2) showed that no QTLs specifically affecting either the face or the anterior cranial fossa. Previous work by Leamy et al. (1999) using linear distances detected 26 QTLs with a predominant effect on either the cranial vault (late developmental modules) or the face (early developmental modules). We also observed a similar dichotomy with a high variability area (e.g., the cranial vault or the basicranium) and a low variability area (e.g., the anterior part of the ventral side of the skull). The developmental origins and mechanical constraints on the various structures provide an explanation. The cranial vault and the basicranium originate from the neural crest (Couly et al. 1993; Kontges and Lumsden 1996) and are under low mechanical constraints. In contrast, the palatine and the inferior part maxilla are derived from mesodermic and somitic tissues (Couly et al. 1992) and are imposed by high mechanical pressures of the hypophysis, the optical chiasma, the superior teeth, and the palatine.

A GENETIC BASIS FOR FLUCTUATING ASYMMETRY?

Examination of Procrustes ANOVA and components of variance of FA (Table 4) showed significant variation was localized on the lateral side of the skull and on the palatine bone (Tables 3 and 4). Previous studies using an F2 cross between LG/J × SM/J mice discovered 11 putative QTLs affecting FA on shape mandible (although 9.5 were expected by chance) (Leamy et al. 1997), whereas, alternative analysis with Procrustes superimposition methods, found only 1 QTL (Klingenberg et al. 2001). Two QTLs exhibited a significant epistasis for FA on molar characters (Leamy et al. 2005). Confirmed by those previous studies (Leamy et al. 2000, 2002), the low magnitude of QTLs effects and a relatively small number of individuals per strains allowed only 1 QTL on each side (Table 4). The amount of FA was not significant for those QTLs because of a loss of power with the superimposition, the correction for FA and subtle QTLs effects. Consequently, our results raise the possibility that FA is genetically controlled although further studies with increased statistical power to detect a significant QTL will be required to properly test this.

Previous work by Leamy et al. (2002) showed the predominance of nonadditive effect and the positive role of the epistasis on the genetic control of FA. In our case, genetic dissection of the 66H IRCSs identified a QTL on chromosome 18 for FA. Analysis of the 66H allelic combinations showed epistasic interactions between chromosome 1 and 18 SEG sequences on the ventral side and between chromosomes 18 and 13 on the dorsal side. Consequently, in the context of interspecific crosses, our data confirmed previous findings that nonadditive effects play an important role on the genetic variation for FA.

EPISTATIC PLEIOTROPY AND COVARIATION

An analysis of the covariation between the ventral and the dorsal side (by the 2B-PLS) indicated a significant covariation between both sides of the skull. Consequently, the skull is a strongly integrated structure. For example, the SEG segments in 137G or 122C strains induced overall shape changes on both sides and were correlated. Interestingly, SEG segments in the strains 120C or 66H produced shape changes on both sides (Figs. S1 and S2). Variations were in the opposite direction on each side resulting in covariations similar to C57BL/6 (Fig. 7A). Moreover, the direction of the covariation between the dorsal and the ventral side was positive (e.g., in direction to SEG), but did not correlate with SEG segment length or number of genes.

Analysis of allelic combinations of the 66H strain led us to explore these mechanisms in more detail. CVA and MANOVA testing of allelic combinations of 66H strain showed an epistatic effect of the B6-Chr 1 by the 66H-Chr18 on the dorsal side and the B6-Chr18 by the B6-Chr1 on the ventral side by the bicongenic strain 66H-Chr1+18 (Figs. 5 and 6). Moreover, we showed an epistatic effect of the 66H-Chr 1 by the 66H-Chr13 on the dorsal side and the 66H-Chr13 by the 66H-Chr1 on the ventral side by the bicongenic strain 66H-Chr1+13 (Figs. 5 and 6). Epistasis between loci was evident for most of the cases (except for the association 66H-Chr1+13 on the dorsal side), a reinforcing of the strongest allele effects (e.g., in a direction of SEG alleles). These results were consistent with previous studies on epistasis (Wolf et al. 2005, 2006). Analysis of the pattern of the covariation between the both sides of the allelic combinations of 66H strain using 2B-PLS showed that 66H-Chr1+18 had a similar pattern as 66H-Chr1 and 66H-Chr13+18 did not differ from 66H-Chr18. In contrast, we observed that the bicongenic strain 66H-Chr1+13 presented an intermediate phenotype between 66H-Chr1 and 66H-Chr13. In this case, the direction of covariation was also linked to the strongest allele effect (e.g., chromosome 1 for the bicongenic strain 66H-Chr1+18 or chromosome 18 for the bicongenic strain 66H-Chr13+18) (Fig. 7B). In accordance with Wolf et al. (2005), the direction of the pleiotropy was mostly positive (e.g., in the direction of SEG allele), except for the bicongenic strain 66H-Chr13+18. Our results are also inline with those of Cheverud et al. (2004) for the mouse mandible, and highlight the role of differential epistasis in the genetic variation of the morphological integration.

Conclusion

Our study using lines derived from a cross between mice of distantly related species, namely *Mus spretus* SEG strain and the most commonly found *Mus musculus* laboratory strain C57BL/6, provided a powerful approach to identify QTLs influencing skull shape, FA, as well as patterns of pleotropy and epistasis. The results revealed that a probable large number of QTLs are likely to be involved in the genetic architecture of skull shape variation. The skull is a highly integrated structure and covariance between traits was evident, predominantly, in the direction of the SEG strain. In addition pleiotropic and epistasic effects on the skull were also oriented towards the SEG strain. In the future work, further crosses and gene expression analysis should give additional insights into the genetic control of variation in morphological integration.

ACKNOWLEDGMENTS

We are very grateful to Isabelle Lanctin for careful breeding of the IRCS, crosses, genotyping, and technical help; Marek Szatanik for genotyping and breeding help; Raphael Cornette and morphometrics platform of the Museum National d'Histoire Naturelle, Paris for skull preparation and technical help; Brendan McMorran for critical reading of the manuscript; and Nicolas Navarro, Christian Klingenberg, and the editor for helpful comments and excellent suggestions on this manuscript to improve its quality.

LITERATURE CITED

Albertson, R. C., J. T. Streelman, T. D. Kocher, and P. C. Yelick. 2005. Integration and evolution of the cichlid mandible: the molecular basis of alternate feeding strategies. Proc. Natl. Acad. Sci. USA 102:16287–16292.

Bastir, M., and A. Rosas. 2005. Hierarchical nature of morphological integration and modularity in the human posterior face. Am. J. Phys. Anthropol. 128:26–34.

Beldade, P., P. M. Brakefield, and A. D. Long. 2002. Contribution of distal-less to quantitative variation in butterfly eyespots. Nature 415:315–318.

Bookstein, F. L. 1991. Morphometric tools for landmarks data: geometry and Biology. Cambridge University Press, New York.

———. 1996. Combining the tools of geometric morphometrics. Pp. 131–151 *in* L. F. Marcus, M. Corti, A. Lov, G. J. P. Naylor, and D. E. Slice, eds. Advances in Morphometrices. NATO ASI Series A vol 284. Plenum, New York.

Bookstein, F. L., P. Gunz, P. Mitteroecker, H. Prossinger, K. Schaefer, and H. Seidler. 2003. Cranial integration in Homo: singular warps analysis of the midsagittal plane in ontogeny and evolution. J. Hum. Evol. 44:167–187.

Breen, M., L. Deakln, B. Macdonald, S. Miller, R. Sibson, E. Tarttelln, P. Avner, F. Bourgade, J.-L. Guenet, X. Montagutelli, et al. 1994. Towards high resolution maps of the mouse and human genomes—a facility for ordering markers to 0.1 cM resolution. Hum. Mol. Genet. 3:621–627.

Breuker, C. J., J. S. Patterson, and C. P. Klingenberg. 2006. A single basis for developmental buffering of *Drosophila* wing shape. Plos. one 1:e7.

Burgio, G., M. Szatanik, J. L. Guenet, M. R. Arnau, J. J. Panthier, and X. Montagutelli. 2007. Interspecific recombinant congenic strains between C57BL/6 and mice of the Mus spretus species : a powerful tool to dissect genetic control of complex traits. Genetics 177:2321–2334.

Cheverud, J. M., E. J. Routman, and D. J. Irschick. 1997. Pleiotropic effects of individual gene loci on mandibular morphology. Evolution 51:2006–2016.

Cheverud, J. M., T. H. Ehrich, T. T. Vaughn, S. F. Koreishi, R. B. Linsey, and L. S. Pletscher. 2004. Pleiotropic effects on mandibular morphology II: differential epistasis and genetic variation in morphological integration. J. Exp. Zool. B Mol. Dev. Evol. 302:424–435.

Couly, G. F., P. M. Coltey, and N. M. Le Douarin. 1992. The developmental fate of the cephalic mesoderm in quail-chick chimeras. Development 114:1–15.

———. 1993. The triple origin of skull in higher vertebrates: a study in quail-chick chimeras. Development 117:409–429.

Demant, P., and A. A. Hart. 1986. Recombinant congenic strains—a new tool for analyzing genetic traits determined by more than one gene. Immunogenetics 24:416–422.

Dryden, I. L., and K. V. Mardia. 1998. Statistical shape analysis. John Wiley and Sons, Chichester, UK.

Ehrich, T., T. T. Vaughn, S. F. Koreishi, R. B. Linsey, L. S. Pletscher, and J. M. Cheverud. 2003. Pleiotropic effects on mandibular morphology I. Developmental morphological integration and differential dominance. J. Exp. Zoolog. B Mol. Dev. Evol. 296:58–79.

Friess, M., and M. Baylac. 2003. Exploring artificial cranial deformation using elliptic Fourier analysis of Procrustes aligned outlines. Am. J. Phys. Anthropol. 122:11–22.

Guenet, J. L., and F. Bonhomme. 2003. Wild mice: an ever-increasing contribution to a popular mammalian model. Trends Genet. 19:24–31.

Guenet, J. L., and X. Montagutelli. 1994. The contribution of wild specimens to the establishment of the mouse genetic map, pp. 285–298. Japan Scientific Society Press, Tokyo.

Gunz, P., and K. Harvati. 2007. The Neanderthal "chignon": variation, integration, and homology. J. Hum. Evol. 52:262–274.

Hallgrimsson, B., J. J. Brown, A. F. Ford-Hutchinson, H. D. Sheets, M. L. Zelditch, and F. R. Jirik. 2006. The brachymorph mouse and the developmental-genetic basis for canalization and morphological integration. Evol. Dev. 8:61–73.

Hallgrimsson, B., D. E. Lieberman, W. Liu, A. F. Ford-Hutchinson, and F. R. Jirik. 2007. Epigenetic interactions and the structure of phenotypic variation in the cranium. Evol. Dev. 9:76–91.

Hemberger, M., H. Kurz, A. Orth, S. Otto, A. Luttges, R. Elliott, A. Nagy, S. S. Tan, P. Tam, U. Zechner, and R. H. Fundele. 2001. Genetic and developmental analysis of X-inactivation in interspecific hybrid mice suggests a role for the Y chromosome in placental dysplasia. Genetics 157:341–348.

Hill, C. A., R. H. Reeves, and J. T. Richtsmeier. 2007. Effects of aneuploidy on skull growth in a mouse model of Down syndrome. J. Anat. 210:394–405.

Ideraabdullah, F. Y., E. de la Casa-Esperon, T. A. Bell, D. A. Detwiler, T. Magnuson, C. Sapienza, and F. P. de Villena. 2004. Genetic and haplotype diversity among wild-derived mouse inbred strains. Genome Res. 14:1880–1887.

Kelsey, J. L., A. S. Whittemore, A. S. Evans, and W. D. Thompson. 1996. Methods in observational epidemiology. Oxford Univ. Press, New York.

Klingenberg, C. P., and G. S. McIntyre. 1998. Geometric morphometrics of developmental instability: analyzing patterns of fluctuating asymmetry with Procrustes methods. Evolution 52:1363–1375.

Klingenberg, C. P., and L. R. Monteiro. 2005. Distances and directions in multidimensional shape spaces: implications for morphometrics applications. Syst. Biol. 54:678–688.

Klingenberg, C. P., M. Barluenga, and A. Meyer. 2002. Shape analysis of symmetric structures: quantifying variation among individuals and asymmetry. Evolution Int. J. Org. Evol. 56:1909–1920.

Klingenberg, C. P., L. J. Leamy, and J. M. Cheverud. 2004. Integration and modularity of quantitative trait locus effects on geometric shape in the mouse mandible. Genetics 166:1909–1921.

Klingenberg, C. P., L. J. Leamy, E. J. Routman, and J. M. Cheverud. 2001. Genetic architecture of mandible shape in mice: effects of quantitative trait loci analyzed by geometric morphometrics. Genetics 157:785–802.

Kontges, G., and A. Lumsden. 1996. Rhombencephalic neural crest segmentation is preserved throughout craniofacial ontogeny. Development 122:3229–3242.

Lachenbruch, P. A., and M. R. Michey. 1968. Estimation of error rates in discriminant analysis. Technometrics 10:1–10.

Lande, R. 1979. Quantitative genetic analysis of multivariate evolution, applied to brain: body size allometry. Evolution 33:402–416.

Langlade, N. B., X. Feng, T. Dransfield, L. Copsey, A. I. Hanna, C. Thebaud, A. Bangham, A. Hudson, and E. Coen. 2005. Evolution through genetically controlled allometry space. Proc. Natl. Acad. Sci. USA 102:10221–10226.

Laurie, C. C., J. R. True, J. Liu, and J. M. Mercer. 1997. An introgression analysis of quantitative trait loci that contribute to a morphological difference between *Drosophila simulans* and *D. mauritiana*. Genetics 145:339–348.

Leamy, L., E. J. Routman, and J. M. Cheverud. 1997. A search for quantitative trait loci affecting asymmetry of mandibular characters in mice. Evolution 51:957–969.

———. 1999. Quantitative trait loci for early- and late-developing skull characters in mice: a test of the genetic independence model of morphological integration. Am. Nat. 153:201–214.

Leamy, L. J., D. Pomp, E. J. Eisen, and J. M. Cheverud. 2000. Quantitative trait loci for directional but not fluctuating asymmetry of mandible characters in mice. Genet. Res. 76:27–40.

Leamy, L. J., E. J. Routman, and J. M. Cheverud. 2002. An epistatic genetic basis for fluctuating asymmetry of mandible size in mice. Evolution 56:642–653.

Leamy, L. J., M. S. Workman, E. J. Routman, and J. M. Cheverud. 2005. An epistatic genetic basis for fluctuating asymmetry of tooth size and shape in mice. Heredity 94:316–325.

Liu, J., J. M. Mercer, L. F. Stam, G. C. Gibson, Z. B. Zeng, and C. C. Laurie. 1996. Genetic analysis of a morphological shape difference in the male genitalia of *Drosophila simulans* and *D. mauritiana*. Genetics 142:1129–1145.

Mardia, K. V., F. L. Bookstein, and I. J. Moreton. 2000. Statistical assessment of bilateral symmetry of shapes. Biometrika 87:285–300.

Mezey, J. G., D. Houle, and S. V. Nuzhdin. 2005. Naturally segregating quantitative trait loci affecting wing shape of *Drosophila melanogaster*. Genetics 169:2101–2113.

Min-Oo, G., A. Fortin, M. F. Tam, A. Nantel, M. M. Stevenson, and P. Gros. 2003. Pyruvate kinase deficiency in mice protects against malaria. Nat. Genet. 35:357–362.

Mitteroecker, P., and F. Bookstein. 2007. The conceptual and statistical relationship between modularity and morphological integration. Syst. Biol. 56:818–836.

Moen, C. J., M. A. Van Der Valk, M. Snoek, B. F. van Zutphen, O. von Deimling, A. A. Hart, and P. Demant. 1991. The recombinant congenic strains—a novel genetic tool applied to the study of colon tumor development in the mouse. Mammal. Genome 1:217–227.

Montagutelli, X., R. Turner, and J. H. Nadeau. 1996. Epistatic control of non-Mendelian inheritance in mouse interspecific crosses. Genetics 143:1739–1752.

Monti, L., M. Baylac, and B. Lalanne-Cassou. 2001. Elliptic Fourier analysis of the form of genitalia in two Spodoptera species and their hybrids (Lepidoptera : Noctuidae). Biol. J. . Linn. Soc. 72:391–400.

Morel, L., C. Mohan, Y. Yu, B. P. Croker, N. Tian, A. Deng, and E. K. Wakeland. 1997. Functional dissection of systemic lupus erythematosus using congenic mouse strains. J. Immunol. 158:6019–6028.

Morel, L., B. P. Croker, K. R. Blenman, C. Mohan, G. Huang, G. Gilkeson, and E. K. Wakeland. 2000. Genetic reconstitution of systemic *lupus erythematosus* immunopathology with polycongenic murine strains. Proc. Natl. Acad. Sci. USA 97:6670–6675.

Mott, R., and J. Flint. 2002. Simultaneous detection and fine mapping of quantitative trait loci in mice using heterogeneous stocks. Genetics 160:1609–1618.

Nagase, H., J. H. Mao, J. P. de Koning, T. Minami, and A. Balmain. 2001. Epistatic interactions between skin tumor modifier loci in interspecific (spretus/musculus) backcross mice. Cancer Res. 61:1305–1308.

Newman, T. L., E. Tuzun, V. A. Morrison, K. E. Hayden, M. Ventura, S. D. McGrath, M. Rocchi, and E. E. Eichler. 2005. A genome-wide survey of structural variation between human and chimpanzee. Genome Res. 15:1344–1356.

Olson, E. C., R. L. Miller. 1958. Morphological integration. University of Chicago Press, Chicago

Palmer, A. R., and C. Strobeck. 1986. Fluctuating asymmetry analyses: measurement, analysis patterns. Annu. Rev. Ecol. Syst. 17:391–421.

Rao, C. R., and S. Suryawanshi. 1998. Statistical analysis of shape through triangulation of landmarks: A study of sexual dimorphism in hominids. Proc. Natl. Acad. Sci. USA 95:4121–4125.

Rohlf, F. J. 1999. Shape statistics: procrustes superimpositions and tangent Spaces. J. Class. 16:197–223.

Rohlf, F. J., and M. Corti. 2000. Use of two-block partial least-squares to study covariation in shape. Syst. Biol. 49:740–753.

Santos, J., X. Montagutelli, A. Acevedo, P. Lopez, C. Vaquero, M. Fernandez, M. R. Arnau, M. Szatanik, E. Salido, J. L. Guenet, et al. 2002. A new locus for resistance to gamma-radiation-induced thymic lymphoma identified using inter-specific consomic and inter-specific recombinant congenic strains of mice. Oncogene 21:6680–6683.

Shimizu, T., H. Oikawa, J. Han, E. Kurose, and T. Maeda. 2004. Genetic analysis of crown size in the first molars using SMXA recombinant inbred mouse strains. J. Dent. Res. 83:45–49.

Sokal, R. R., and F. J. Rohlf. 1995. Biometry:the principles and practices of statistics in biological research. W.H. Freeman, and Co., New York.

Valdar, W., L. C. Solberg, D. Gauguier, S. Burnett, P. Klenerman, W. O. Cookson, M. S. Taylor, J. N. Rawlins, R. Mott, and J. Flint. 2006. Genome-wide genetic association of complex traits in heterogeneous stock mice. Nat. Genet. 38:879–887.

van Wezel, T., A. P. Stassen, C. J. Moen, A. A. Hart, M. A. van der Valk, and P. Demant. 1996. Gene interaction and single gene effects in colon tumour susceptibility in mice. Nat. Genet. 14:468–470.

Wade, C. M., E. J. Kulbokas, 3rd, A. W. Kirby, M. C. Zody, J. C. Mullikin, E. S. Lander, K. Lindblad-Toh, and M. J. Daly. 2002. The mosaic structure of variation in the laboratory mouse genome. Nature 420:574–578.

Willmore, K. E., L. Leamy, and B. Hallgrimsson. 2006a. Effects of developmental and functional interactions on mouse cranial variability through late ontogeny. Evol. Dev. 8:550–567.

Willmore, K. E., M. L. Zelditch, N. Young, A. Ah-Seng, S. Lozanoff, and B. Hallgrimsson. 2006b. Canalization and developmental stability in the Brachyrrhine mouse. J. Anat. 208:361–372.

Wolf, J. B., L. J. Leamy, E. J. Routman, and J. M. Cheverud. 2005. Epistatic pleiotropy and the genetic architecture of covariation within early and late-developing skull trait complexes in mice. Genetics 171:683–694.

Wolf, J. B., D. Pomp, E. J. Eisen, J. M. Cheverud, and L. J. Leamy. 2006. The contribution of epistatic pleiotropy to the genetic architecture of covariation among polygenic traits in mice. Evol. Dev. 8:468–476.

Workman, M. S., L. J. Leamy, E. J. Routman, and J. M. Cheverud. 2002. Analysis of quantitative trait locus effects on the size and shape of mandibular molars in mice. Genetics 160:1573–1586.

Yang, H., T. A. Bell, G. A. Churchill, and F. Pardo-Manuel de Villena. 2007. On the subspecific origin of the laboratory mouse. Nat. Genet. 39:1100–1107.

Young, N. M., S. Wat, V. M. Diewert, L. W. Browder, and B. Hallgrimsson. 2007. Comparative morphometrics of embryonic facial morphogenesis: implications for cleft-lip etiology. Anat. Rec. (Hoboken) 290:123–139.

Zechner, U., M. Reule, A. Orth, F. Bonhomme, B. Strack, Guenet, H. Hameister, and R. Fundele. 1996. An X-chromosome linked locus contributes to abnormal placental development in mouse interspecific hybrid. Nat. Genet. 12:398–403.

Zeng, Z. B., J. Liu, L. F. Stam, C. H. Kao, J. M. Mercer, and C. C. Laurie. 2000. Genetic architecture of a morphological shape difference between two Drosophila species. Genetics 154:299–310.

Associate Editor: Dr. C. Goodnight

Supporting Information

The following supporting information is available for this article:

Figure S1. Visualization of significant IRCS QTL effects on the dorsal shape.
Figure S2. Visualization of significant IRCS QTL effects on the ventral shape.
Figure S3. Visualization of FA shape deformations on the dorsal and ventral side for the 66H-Chr18 strain.
Table S1. Statistics of 2B-PLS analyses with all significant correlations between PLS axes (under 1000 permutations).

Supporting Information may be found in the online version of this article.
(This link will take you to the article abstract).

Please note: Wiley-Blackwell are not responsible for the content or functionality of any supporting information supplied by the authors. Any queries (other than missing material) should be directed to the corresponding author for the article.
Additional results and discussion can be found in a document at http://www.repository.naturalis.nl/record/289893.